tvst

Article

Quantification of Translaminar Pressure Gradient (TLPG) With Continuous Wireless Telemetry in Nonhuman Primates (NHPs)

Jessica V. Jasien[1], Massimo A. Fazio[2], Brian C. Samuels[2], James M. Johnston[3], and J. Crawford Downs[2]

[1] Vision Science Graduate Program, School of Optometry, The University of Alabama at Birmingham, Birmingham, AL, USA
[2] Department of Ophthalmology and Visual Sciences, School of Medicine, The University of Alabama at Birmingham, Birmingham, AL, USA
[3] Department of Neurosurgery, School of Medicine, The University of Alabama at Birmingham, Birmingham, AL, USA

Correspondence: J. Crawford Downs, Department of Ophthalmology and Visual Sciences, School of Medicine, The University of Alabama at Birmingham, 390B Volker Hall, 1670 University Boulevard, Birmingham, AL 35294, USA. e-mail: cdowns@uabmc.edu

Received: July 27, 2020
Accepted: October 10, 2020
Published: November 12, 2020

Keywords: intraocular pressure; intracranial pressure; translaminar pressure; translaminar pressure gradient; nonhuman primate

Citation: Jasien JV, Fazio MA, Samuels BC, Johnston JM, Downs JC. Quantification of translaminar pressure gradient (TLPG) with continuous wireless telemetry in nonhuman primates (NHPs). Trans Vis Sci Tech. 2020;9(12):18, https://doi.org/10.1167/tvst.9.12.18

Purpose: Recent retrospective clinical and animal studies suggest that cerebrospinal fluid pressure (CSFP) is important in glaucoma pathogenesis. Intraocular pressure (IOP) and CSFP are the driving components of translaminar pressure (TLP = IOP – CSFP), which acts across the lamina cribrosa (LC) thickness to create the translaminar pressure gradient (TLPG = TLP/LC thickness).

Methods: We developed an implantable wireless telemetry system based on a small piezoelectric sensor with low temporal drift. IOP, measured in the anterior chamber, and intracranial pressure (ICP), measured in the brain parenchyma (as a surrogate for CSFP) were measured at 200 Hz in three male rhesus macaques (nonhuman primates, NHPs) on a 10% duty cycle (15 seconds of every 150-second period). Three-dimensional LC thickness was autosegmented as the mean thickness of the visible hyperreflective band in 48 radial spectral-domain optical coherence tomography b-scans centered on the optic nerve head.

Results: Results indicated the rank order of IOP, ICP, TLP, and TLPG for waking, sleeping, and 24-hour periods averaged across all days. NHP 150110 had the highest IOP and ICP in all periods; however, it had the lowest TLPG in all periods due to its relatively thick LC. The other two NHPs showed similar shifts in the rank order of possible glaucoma risk factors.

Conclusions: IOP is the only modifiable and readily measurable pressure-based risk factor for glaucoma. However, other potential risk factors such as ICP, TLP, and TLPG, as well as their rank-order patterns, differed compared to IOP across subjects, demonstrating that a comprehensive view of relevant risk factors is warranted.

Translational Relevance: Future studies should consider including CSFP, TLP, and TLPG in addition to IOP as potential risk factors when assessing eye-specific glaucoma susceptibility.

Introduction

Intraocular pressure (IOP) is a primary risk factor for glaucoma, and lowering IOP is the only proven treatment for the disease; however, the mechanisms of glaucomatous optic nerve injury are not fully understood. Optic nerve head (ONH) biomechanics, which are the physical manifestations of the force distribution in the tissues, are thought to be important to glaucoma pathophysiology.[1–3] However, to our knowledge, no studies to date have directly linked ONH biomechanics to disease in human patients or fully elucidated the pathways through which mechanical stress and strain damages the retinal ganglion cell axons as they pass through the ONH. Although there are many studies suggesting that ONH biomechanics[3–5] and remodeling[6–13] are important in glaucoma, other aspects of

ocular physiology, such as vascular compromise,[14–16] metabolic deficiency,[17–19] and general neurodegeneration,[20] likely contribute to the eye-specific risk of glaucoma development and/or progression. Although the biomechanical framework of glaucoma seemingly focuses on IOP, cerebrospinal fluid pressure (CSFP), and tissue strain, it also encompasses the vascular and cellular pathways of axonal damage.[21] For example, blood flow is reduced in intrascleral vessels and intraocular capillaries under increased IOP and/or strain,[5] and increased variable cyclic mechanical strain alters cell metabolism via mechanotransduction in many cell types, including vascular endothelial cells.[22–24]

It has been hypothesized that CSFP is a driving factor in glaucoma, as it provides a counter-pressure to IOP, but only at the ONH.[25–41] Although IOP acts on the entire globe and affects ONH biomechanics through both laminar and scleral canal stress and strain, CSFP only acts as a retrolaminar pressure. CSFP effects are therefore limited to the ONH and contained lamina cribrosa (LC). Given this interplay of pressures acting on the ONH, it is plausible that the translaminar pressure (TLP = IOP – CSFP) is more relevant to glaucoma than either IOP or CSFP alone, although IOP and CSFP may affect the ONH differently according to some numerical simulations[36] and experimental studies.[42] It is also important to note that TLP is different from the translaminar pressure gradient (TLPG = TLP/laminar thickness), which is the pressure gradient acting across the thickness of the lamina cribrosa. TLPG captures additional structural information that may also prove relevant to glaucoma. Although snapshot IOP measurements can be performed noninvasively in the clinic, CSFP assessment is generally accomplished through lumbar puncture in the lateral decubitus position or measuring intracranial pressure (ICP) with an intraparenchymal sensor. As a result, little is known about either IOP or CSFP dynamics; however, continuous measurement of TLP fluctuations may provide insight into the mechanisms underlying glaucoma pathogenesis and/or progression.

Recent retrospective clinical studies and animal experiments have suggested that higher CSFP (measured with a single lumbar puncture) is protective against glaucoma, and low CSFP increases glaucoma risk.[27,29] Prospective studies have found that CSFP decreases with age and is lower in patients with primary open-angle glaucoma and normal-tension glaucoma compared to healthy controls or patients with ocular hypertension.[37,43] However, TLP estimates in these reports are extrapolated because the CSFP and IOP measurements occurred at different time points, sometimes months apart.[26] In addition, very little is known about TLP dynamics, as characterization of the true, 24-hour TLP exposure in individual eyes has not been possible due to the lack of accurate, continuous measurement of both IOP and CSFP in patients or large animal models of glaucoma, such as nonhuman primates (NHPs). Changes in IOP, CSFP, and TLP occur frequently and at multiple time scales; yet, it is not known if these fluctuations impact glaucoma development and/or progression.[40,41,44]

There are currently no science-based tools to predict the IOP and/or TLP/TLPG levels at which an individual's ONH will be damaged or what levels lead to progression when disease onset has occurred. Understanding the relationships among IOP, CSFP, TLP, and TLPG and their fluctuations will drive the clinical assessment of safe target IOP, TLP, and/or TLPG. Although IOP is easily measured and therapeutically altered, retrobulbar CSFP can only be estimated. To address this gap in knowledge, we have developed and validated a fully implantable, wireless telemetry system (TSE Systems Stellar, Chesterfield, MO) that can measure IOP and intracranial pressure at the level of the eye (a surrogate measure of CSFP) continuously in NHPs to elucidate the IOP, CSFP, TLP, and TLPG dynamics over long periods.[45] The purpose of this preliminary study was to assess the differences in IOP, TLP, and TLPG and their rank order among NHPs to demonstrate stratification of potential glaucoma risk factors.

Methods

Animals

All animals were treated in accordance with the ARVO Statement for the Use of Animals in Ophthalmic and Vision Research under an approved Institutional Animal Care and Use Committee protocol monitored by the University of Alabama at Birmingham. Three male rhesus macaques, 4.5 to 6.5 years old (Table 1), with no ocular abnormalities, were used in this study. All animals were kept on a 6:00 AM/6:00 PM light/dark cycle and fed daily at approximately 6:00 AM and 2:00 PM, with water available ad libitum through a continuous feed. Food and water intake were not monitored.

Stellar IOP, ICP, and Arterial BP Telemetry System

We have developed and validated an implantable pressure telemetry system based on a small piezoelectric transducer with low temporal drift that accurately

Table 1. Animal Demographics

NHP	Age, y	Sex	Number of Days of IOP and ICP Telemetry Monitoring	Number of OCT Imaging Sessions
150069	4.5	Male	69	8
12.38	6.5	Male	88	3
150110	4.5	Male	281	9

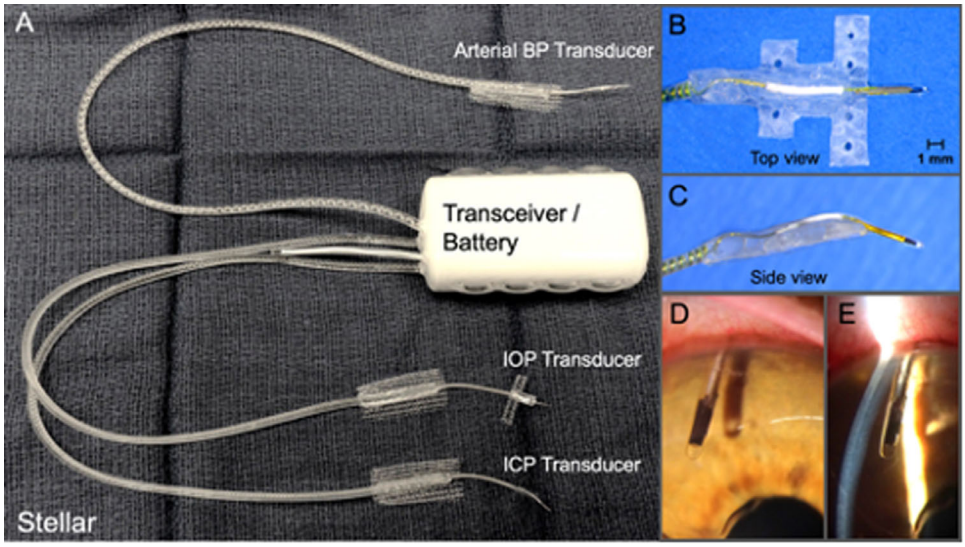

Figure 1. (A) TSE Systems Stellar IOP/ICP/BP total implant system. (B) Top view of the IOP transducer and integrated scleral baseplate for affixing the transducer to the sclera under Tenon's capsule and conjunctiva. (C) Side view of the IOP transducer and integrated scleral baseplate. (D) En face photograph of the piezoelectric IOP transducer in the anterior chamber. (E) Slit-lamp photograph of the intraocular placement of the piezoelectric IOP transducer in the anterior chamber relative to the cornea and iris. Reprinted with permission from Jasien et al.[45]

measures IOP in the anterior chamber, ICP in the parenchyma of the brain (as a surrogate for CSFP), and arterial blood pressure (BP) in the lumen of a major artery (data not shown) (Fig. 1).[45] As previously described by our group, the IOP transducer was placed in the anterior chamber of the right eye and the ICP transducer was placed in the right frontal lobe, ~2.5 cm from the midline of the brain at the same height as the IOP transducer when the animal is upright (Fig. 1).[45] The telemetry system wirelessly records 200 measurements of each physiologic pressure per second on a 10% duty cycle (15 seconds of every 150-second period), 24 hours per day. An in-depth description of the surgical procedure and placement of the wireless telemetry implant and each pressure transducer has been previously described in our recent study describing the diurnal cycle of TLP.[45]

IOP and ICP Calibration

Anesthesia was induced using ketamine (3 mg/kg) with dexmedetomidine (50 µg/kg via intramuscular injection) and maintained using inhaled isoflurane (1%–3%) for ONH imaging and transducer calibrations. Proparacaine hydrochloride (0.5% ophthalmic solution) was applied to anesthetize the cornea prior to anterior chamber cannulation. During all calibration procedures, the NHPs were kept warm with a warming blanket and systemically monitored for heart rate, oxygen saturation, end-tidal CO_2 volume, electrocardiogram, and temperature, with documentation every 15 minutes.

As previously described, the IOP telemetry transducer was calibrated every 2 weeks via anterior chamber cannulation manometry with a 27-gauge needle placed through the cornea at the limbus under slit-lamp biomicroscopy.[45] To assess the error in the IOP transducer reading, absolute manometric IOP is elevated from 5 to 30 mm Hg in 5-mm Hg steps. All IOP data are corrected for signal drift between calibrations using the 15-mm Hg value; transducer drift is approximately 2 mm Hg a month.

The ICP telemetry transducer was calibrated once a month in the same session as the biweekly IOP telemetry transducer calibration. As previously described, a

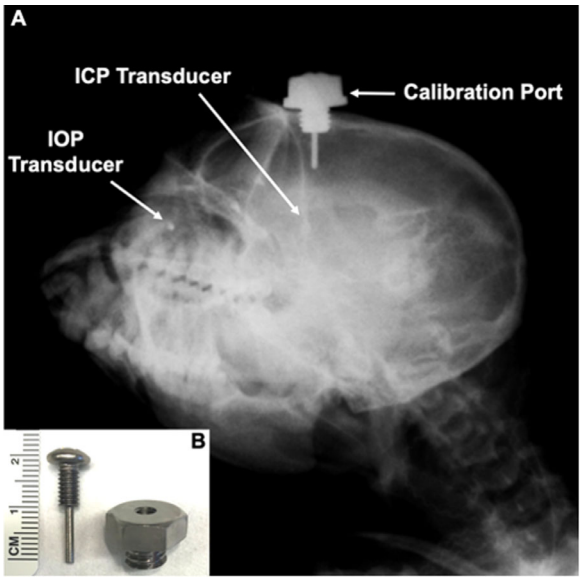

Figure 2. (A) Oblique x-ray of an NHP with the Stellar implant (IOP and ICP transducers) and custom indwelling titanium ICP calibration port installed. The IOP transducer is in the right eye, and the ICP transducer is in the right lobe of the brain, whereas the calibration port is in the left lobe. The IOP and ICP transducers and bottom of the screw post within the calibration port are at the same height when the animal's head is in the upright position. (B) Photograph of the custom indwelling titanium ICP calibration port, showing the bolt with central screw. Note that the screw is sealed to the bolt with a sterile medical-grade silicone washer when installed. Reprinted with permission from Jasien et al.[45]

clinical gold-standard Codman ICP Express microsensor (DePuy Synthes Companies, Raynham, MA) was inserted through an indwelling custom titanium port in the cranium that allows access to the left brain parenchyma (Fig. 2).[45] ICP was then measured by both the indwelling Stellar telemetry transducer and the Codman microsensor simultaneously at various body positions.[45] The prone position was used as the calibration reference for all calibration sessions (Fig. 3).[45] ICP transducer drift was similar to IOP transducer drift at approximately 2 mm Hg per month, and calibrated TLP was continuously quantified as IOP – ICP. All IOP and ICP data were recorded with NOTOCORD-hem data acquisition software (Instem, Staffordshire, UK), and all pressure data were drift-corrected continuously between calibration procedures via software postprocessing assuming linear drift between calibrations.

In Vivo Imaging and Quantification of LC Thickness

Spectral-domain optical coherence tomography (SD-OCT; Spectralis 2, Heidelberg Engineering, Heidelberg, Germany) images through the ONH of each NHP were obtained monthly for the duration of the study, resulting in three to nine imaging sessions per animal. In each imaging session, 48 radial, high-resolution b-scans centered in the ONH were acquired in follow-up mode for each eye at an IOP of 10 mm Hg. IOP was set to 10 mm Hg by anterior chamber manometry and allowed to stabilize for 10 minutes prior to imaging.

Automated image processing of the OCT scans was used to reduce noise, enhance contrast, and automatically segment the LC. The LC was defined as the hyperreflective band of tissue visible in each radial OCT scan. The automated segmentation algorithm operates by searching in the center of the scan volume for a continuous set of voxels with high light-intensity values. It then grows the targeted region by iteratively minimizing a three-dimensional (3D) functional form of the light intensity that is a weighted sum of the contour length, the enclosed area, and the deviation between the image and the two-level segmentation.[46] This is a particularly effective approach in NHPs because their thinner prelaminar tissues allow for much deeper penetration of the OCT scanning beam in the ONH region. A sharp decrease in reflectivity is typically present 100 to 200 µm below the anterior LC surface, which is segmented as the posterior LC surface (Fig. 4). LC thickness was calculated as the average distance between the anterior and posterior 3D LC surfaces. Two-dimensional projections of the anterior and posterior surfaces were overlaid on each b-scan and then manually reviewed. An overlaid view of the segmentation for the nasal–temporal SD-OCT b-scan of all nine 48 radial scans taken at 10 mm Hg IOP from NHP 150069 is provided in Figure 5; similar figures are provided in the Supplementary Material for all scans at 10 mm Hg IOP for all NHPs (Supplementary Figs. S1–S3).

Statistical Analysis

One-way analyses of variance were used to determine if IOP, ICP, TLP, and TLPG were different across NHPs within each time period (wake, sleep, and 24-hour) and to determine the difference in LC thickness across NHPs. In order to test the reproducibility of quantifying LC thickness by autosegmentation, we assessed the intra- and intersubject variability of the LC thickness across imaging sessions (4 weeks apart). *F*-test significance was computed as the LC thickness variance between animals divided by the variance across imaging sessions (error term).

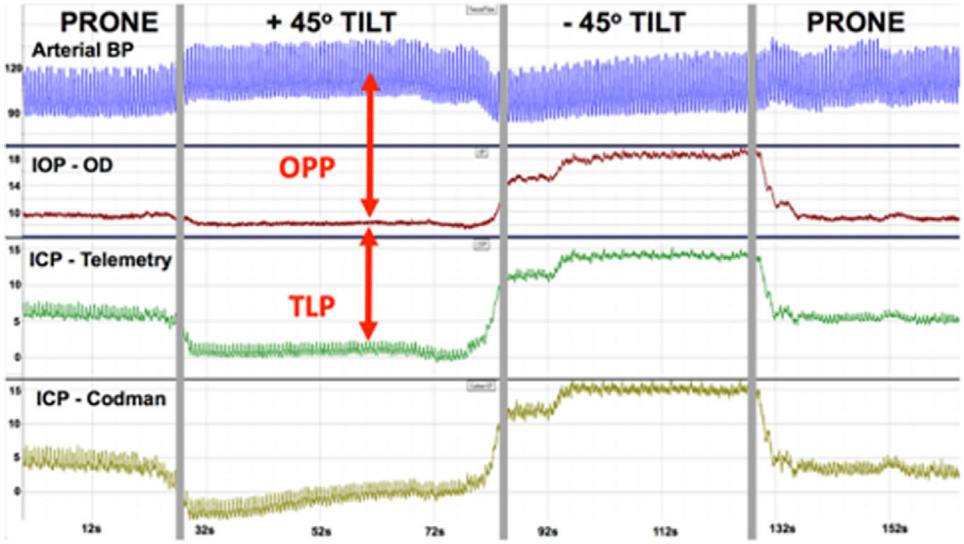

Figure 3. Screenshot of the pressure telemetry signals acquired during a typical ICP transducer calibration procedure wherein the NHP is moved from the prone position to a positive 45° incline (head up) to a negative 45° decline (head down) and back to prone. Arterial BP (*blue*), IOP in the right eye (*red*), ICP from Stellar Telemetry (*green*), and ICP from the Codman microsensor (*gold*) are recorded at 200 Hz during the calibration procedure. The *y*-axis scale is mm Hg for all signals. Reprinted with permission from Jasien et al.[45]

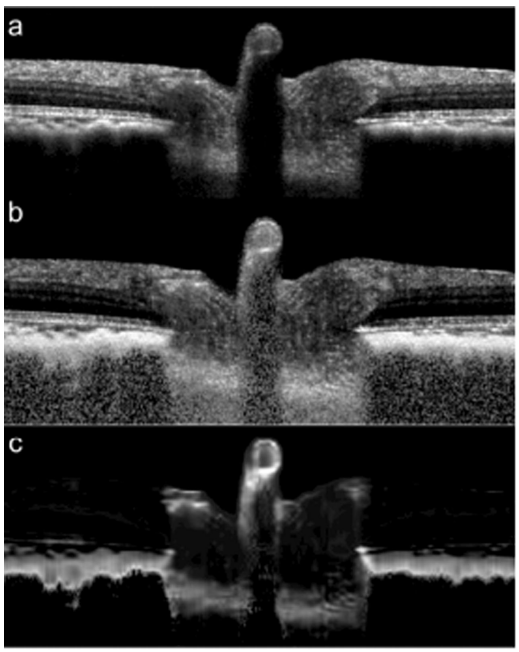

Figure 4. (a) Unprocessed SD-OCT reflectance radial b-scan through the ONH in a NHP. (b) The original scan after custom filtering and deep tissue enhancement. (c) The original scan after principal light intensity curvature computation to enhance the different layers of the tissue; the hyperreflective band defining the LC is clearly visible, and LC autosegmentation is shown in Figure 5.

Results

Translaminar Pressure Gradient

The rank order of IOP, ICP, TLP, and TLPG for the waking, sleeping, and 24-hour periods averaged across all days is shown in Table 2. Although NHP 150110 has the highest IOP and ICP in all periods, it had the lowest TLPG in all periods due to its relatively thick LC. Similar shifts in the rank order of possible glaucoma risk factors were also observed for the other two NHPs. Also, note the relatively small standard deviations, showing low variability and excellent repeatability in all measures. IOP, ICP, TLP, and TLPG were significantly different among the NHPs in the wake, sleep, and 24-hour periods ($P < 0.0001$), except for the TLP 24-hour period ($P = 0.7$).

Repeatability of the LC Thickness Autosegmentation

Descriptive statistics of LC thickness variation across animals and IOP are summarized by means and standard deviations in Table 2. Intra- and intersubject variability quantification showed that, across animals, variation of LC thickness (thickness of the hyperreflective band) was significantly larger (NHPs, F-ratio = 96.46) than its variability across imaging sessions ($P < 0.001$) (Table 3).

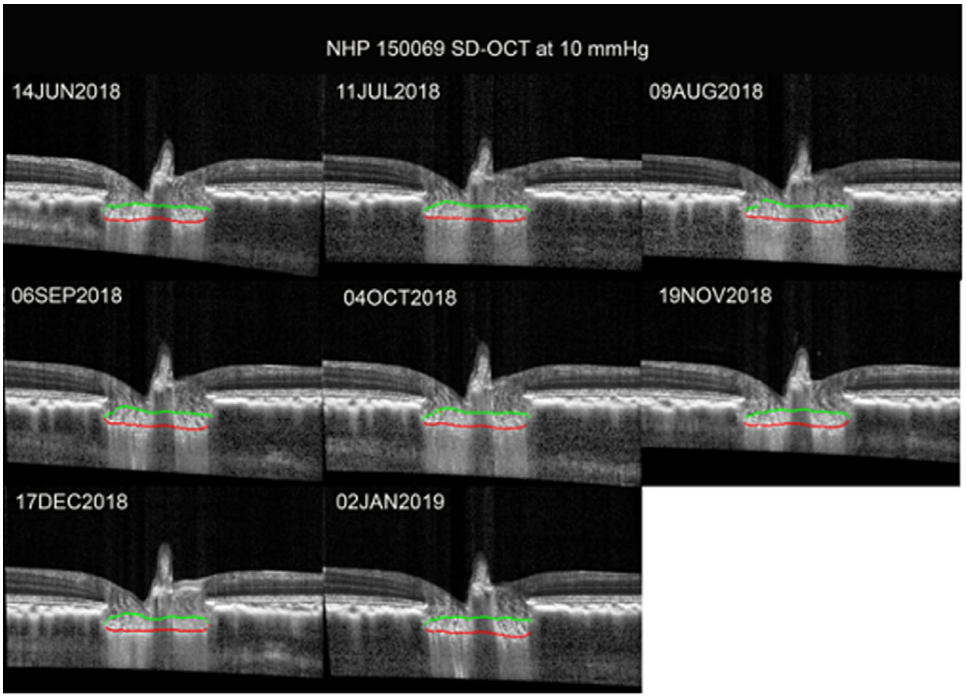

Figure 5. Lamina cribrosa thickness (µm) in the nasal–temporal b-scans through the ONH in all eight sessions, 1 month apart, for NHP 150069 at an IOP of 10 mm Hg.

Table 2. Average IOP, ICP, TLP, and TLPG for the Waking (6:00–18:00), Sleeping (18:00–6:00), and 24-Hour Periods Across All Days by NHP, Presented in Color-Coded Rank Order[a]

	Mean ± SD		
Parameter/NHP	**150069**	**12.38**	**150110**
IOP, mm Hg			
Waking	12.9 ± 0.6	15.5 ± 0.4	15.9 ± 0.6
Sleeping	13.6 ± 0.5	15.4 ± 0.6	17.8 ± 0.8
24-Hr	13.2 ± 0.6	15.4 ± 0.5	16.8 ± 1.2
ICP, mm Hg			
Waking	2.4 ± 0.6	3.4 ± 1.9	5.3 ± 0.6
Sleeping	6.4 ± 0.6	8.9 ± 1.2	10.2 ± 1
24-Hr	4.3 ± 2.1	6.2 ± 3.2	7.8 ± 2.6
TLP, mm Hg			
Waking	10.5 ± 0.9	12.0 ± 1.9	10.5 ± 1
Sleeping	7.2 ± 0.3	6.5 ± 0.9	7.6 ± 0.3
24-Hr	8.9 ± 1.8	9.1 ± 3	9.0 ± 1.7
TLPG, mm Hg/µm			
Waking	0.087 ± 0.004	0.145 ± 0.015	0.054 ± 0.005
Sleeping	0.059 ± 0.003	0.079 ± 0.008	0.039 ± 0.004
24-Hr	0.073 ± 0.04	0.110 ± 0.011	0.046 ± 0.005
LC thickness, µm	121 ± 6.4	83 ± 9.0	196 ± 18.6

[a]Rank order: green, lowest; yellow, middle; red, highest.

Discussion

In this preliminary study, IOP and ICP data were collected in three male rhesus macaques on a 10% duty cycle, consisting of 200 measurements per second captured for 15 seconds of every 150-second period over a range of 69 to 281 days. TLPG measurements were calculated as (IOP – ICP)/LC thickness, defined as the overall mean thickness of the hyperreflective band

Table 3. *F*-Ratio Values for LC Thickness Variability Across NHPs and Imaging Sessions

Variable	Mean Square	*F*-Ratio	*P*
NHPs	37,815.98	96.46	<0.001
Imaging session	392.04	1.00	0.50
Error	586.74	1.50	0.21
Total	2515.68	6.42	0.00

within 48 radial SD-OCT image sets taken through the center of the ONH. Outcomes from the *F*-ratio analyses show that the hyperreflective band thickness in OCT was repeatable and therefore adequate for detecting the eye-specific variability in LC thickness. We have focused on eye-specific responses to IOP and TLP/TLPG that could contribute to glaucomatous pathophysiology. The purpose of this study was to assess the differences in IOP, TLP, and TLPG and their rank order among NHPs to demonstrate stratification of potential glaucoma risk factors. Results show that other potential risk factors such as ICP/CSFP, TLP, and TLPG, as well as their rank-order patterns, differ compared to IOP across subjects, demonstrating that a comprehensive view of relevant risk factors is warranted.

There is a strong and consistent diurnal cycle in ICP and TLP in NHPs, wherein TLP is much higher during waking hours in four NHPs,[45] and this pattern matches that reported for humans.[47] Importantly, the diurnal cycle of TLP is driven primarily by CSFP, not IOP, due to the large magnitude of diurnal CSFP changes, further indicating that CSFP plays an important role in ONH biomechanics and may contribute to glaucoma. As mentioned, TLPG takes laminar morphology into account and may be even more relevant to glaucoma than IOP, CSFP, or TLP. Morgan and colleagues[33,35] measured TLPG in dogs and found a strong correlation between the TLPG and TLP when the ICP was greater than 0 mm Hg. Hou and colleagues[48] also showed a positive correlation between ICP and retrolaminar tissue pressure above 3 mm Hg in dogs, although retrolaminar pressure was constant when ICP was less than 3 mm Hg. These studies showed that ICP and retrolaminar pressure are generally similar in dogs; therefore, it is reasonable to use ICP as a surrogate for CSFP when quantifying TLP in NHPs, as done in this study. We have recently shown that both ICP and TLP exhibit a large nychthemeral rhythm in spite of the fact that NHPs sleep sitting up, with TLP showing a 4.2-mm Hg (56%) mean increase during waking hours compared to sleeping hours.[45] A similar relative increase in ICP has been reported in humans when moving from the upright to supine position.[49] Unlike humans, NHPs sleep upright, so the large diurnal cycle in ICP and TLP was somewhat unexpected; the source of this nocturnal ICP increase is still being investigated in our laboratory.

The most striking finding in the current study is that the rank order of TLPG in these NHPs, which takes the laminar structure into account and may be even more relevant to glaucoma than IOP, CSFP, or TLP, is completely different from the order of these potential risk factors. Ample evidence suggests that higher IOP increases glaucoma risk. If one presumes that higher TLP and/or higher TLPG also increases glaucoma risk, then stratifying the three NHPs in this study by potential risk using a single variable is problematic, as shown in Table 2. In fact, the NHP with the highest IOP is also the animal with the lowest TLPG, demonstrating that a more comprehensive view of the possible glaucoma risk factors is warranted. Further study of the contributions of IOP, TLP, and TLPG to glaucoma risk are needed.

The study is limited by the following considerations. First, the study was limited to a small sample size of three NHPs due to the preliminary nature of the investigation; hence, the reported results may not translate to the larger population of Rhesus macaques, although the results were significantly different among animals across time periods and thus we had adequate statistical power to detect effects. Future studies should be sure to include a larger sample size. Also, these results may not translate to the human population, although similar differences in LC thickness have been reported among patients,[50,51] so it is likely that similar variability in TLPG would be present across patients. Second, the repeatability of the number of scans was a closer confidence interval in the animals with more OCT sessions. The repeatability of the segmentation of the LC thickness measurements as the hyperreflective band has to be validated with a larger study and the use of histological measurements, as it is known that posterior identification of the LC using OCT is challenging.

IOP is the only modifiable and readily measurable pressure-based risk factor for glaucoma, but other potential risk factors such as ICP, TLP, and TLPG may differ compared to IOP across subjects, demonstrating that a comprehensive view of relevant risk factors is warranted. Future studies should consider including CSFP, TLP, and TLPG in addition to IOP as potential risk factors when assessing eye-specific glaucoma susceptibility.

Acknowledgments

The authors express their sincerest appreciation to Cheryl Killingsworth, DVM, PhD, Dipl ACVS, for her

surgical expertise and assistance; Lisa Hethcox, LVT, and Candice Jackson, LVT, for their invaluable help in the both data acquisition and the care and handling of the NHPs; and Chester Calvert and Ryan Whitley for their invaluable assistance in data export and filtering.

Supported by a Grant from the BrightFocus Foundation (G2016165, JCD); by a core grant from the National Eye Institute, National Institutes of Health (P30 EY003039, BCS); by the EyeSight Foundation of Alabama (unrestricted departmental funds); and by Research to Prevent Blindness (unrestricted departmental funds).

Disclosure: **J.V. Jasien**, None; **M.A. Fazio**, None; **B.C. Samuels**, None; **J.M. Johnston**, None; **J.C. Downs**, None

References

1. Zeimer R. Biomechanical properties of the optic nerve head. In: Drance SM, ed. *Optic Nerve in Glaucoma*. Amsterdam: Kugler Publications; 1995:107–121.
2. Quigley H, Addicks E. Regional differences in the structure of the lamina cribrosa and their relation to glaucomatous optic nerve damage. *Arch Ophthalmol*. 1981;99(1):137–143.
3. Downs JC. Optic nerve head biomechanics in aging and disease. *Exp Eye Res*. 2015;133:19–29.
4. Burgoyne CF. A biomechanical paradigm for axonal insult within the optic nerve head in aging and glaucoma. *Exp Eye Res*. 2011;93(2):120–132.
5. Burgoyne CF, Downs JC, Bellezza AJ, Suh JK, Hart RT. The optic nerve head as a biomechanical structure: a new paradigm for understanding the role of IOP-related stress and strain in the pathophysiology of glaucomatous optic nerve head damage. *Prog Retin Eye Res*. 2005;24(1):39–73.
6. Downs JC, Yang H, Girkin CA, et al. Three-dimensional histomorphometry of the normal and early glaucomatous monkey optic nerve head: neural canal and subarachnoid space architecture. *Invest Ophthalmol Vis Sci*. 2007;48(7):3195–3208.
7. Yang H, Downs JC, Girkin C, et al. 3-D histomorphometry of the normal and early glaucomatous monkey optic nerve head: lamina cribrosa and peripapillary scleral position and thickness. *Invest Ophthalmol Vis Sci*. 2007;48(10):4597–4607.
8. Yang H, Ren R, Lockwood H, et al. The connective tissue components of optic nerve head cupping in monkey experimental glaucoma part 1: global change. *Invest Ophthalmol Vis Sci*. 2015;56(13):7661–7678.
9. Downs JC, Roberts MD, Sigal IA. Glaucomatous cupping of the lamina cribrosa: a review of the evidence for active progressive remodeling as a mechanism. *Exp Eye Res*. 2011;93(2):133–140.
10. Downs JC, Suh JK, Thomas KA, Bellezza AJ, Hart RT, Burgoyne CF. Viscoelastic material properties of the peripapillary sclera in normal and early-glaucoma monkey eyes. *Invest Ophthalmol Vis Sci*. 2005;46(2):540–546.
11. Roberts MD, Grau V, Grimm J, et al. Remodeling of the connective tissue microarchitecture of the lamina cribrosa in early experimental glaucoma. *Invest Ophthalmol Vis Sci*. 2009;50(2):681–690.
12. Roberts MD, Sigal IA, Liang Y, Burgoyne CF, Downs JC. Changes in the biomechanical response of the optic nerve head in early experimental glaucoma. *Invest Ophthalmol Vis Sci*. 2010;51(11):5675–5684.
13. Ivers KM, Sredar N, Patel NB, et al. In vivo changes in lamina cribrosa microarchitecture and optic nerve head structure in early experimental glaucoma. *PLoS One*. 2015;10(7):e0134223.
14. Cherecheanu AP, Garhofer G, Schmidl D, Werkmeister R, Schmetterer L. Ocular perfusion pressure and ocular blood flow in glaucoma. *Curr Opin Pharmacol*. 2013;13(1):36–42.
15. Cull G, Burgoyne CF, Fortune B, Wang L. Longitudinal hemodynamic changes within the optic nerve head in experimental glaucoma. *Invest Ophthalmol Vis Sci*. 2013;54(6):4271–4277.
16. Wang L, Cull G, Burgoyne CF, Thompson S, Fortune B. Longitudinal alterations in the dynamic autoregulation of optic nerve head blood flow revealed in experimental glaucoma. *Invest Ophthalmol Vis Sci*. 2014;55(6):3509–3516.
17. Bernard K, Logsdon NJ, Ravi S, et al. Metabolic reprogramming is required for myofibroblast contractility and differentiation. *J Biol Chem*. 2015;290(42):25427–25438.
18. Coughlin L, Morrison RS, Horner PJ, Inman DM. Mitochondrial morphology differences and mitophagy deficit in murine glaucomatous optic nerve. *Invest Ophthalmol Vis Sci*. 2015;56(3):1437–1446.
19. Williams PA, Harder JM, Foxworth NE, et al. Vitamin B3 modulates mitochondrial vulnerability and prevents glaucoma in aged mice. *Science*. 2017;355(6326):756–760.
20. Danesh-Meyer HV, Levin LA. Glaucoma as a neurodegenerative disease. *J Neuroophthalmol*. 2015;35(suppl 1):S22–S28.

21. Sigal IA, Roberts MD, Girard MJA, Burgoyne CF, Downs JC. Biomechanical changes of the optic disc. In: Levin LA, Albert DM, eds. *Ocular Disease: Mechanisms and Management*. London: Elsevier; 2010:153–164.
22. Beckel JM, Argall AJ, Lim JC, et al. Mechanosensitive release of adenosine 5′-triphosphate through pannexin channels and mechanosensitive upregulation of pannexin channels in optic nerve head astrocytes: a mechanism for purinergic involvement in chronic strain. *Glia*. 2014;62(9):1486–1501.
23. Bartolak-Suki E, Imsirovic J, Parameswaran H, et al. Fluctuation-driven mechanotransduction regulates mitochondrial-network structure and function. *Nat Mater*. 2015;14(10):1049–1057.
24. Suki B, Parameswaran H, Imsirovic J, Bartolak-Suki E. Regulatory roles of fluctuation-driven mechanotransduction in cell function. *Physiology (Bethesda)*. 2016;31(5):346–358.
25. Jonas JB, Berenshtein E, Holbach L. Anatomic relationship between lamina cribrosa, intraocular space, and cerebrospinal fluid space. *Invest Ophthalmol Vis Sci*. 2003;44(12):5189–5195.
26. Berdahl JP, Allingham RR. Intracranial pressure and glaucoma. *Curr Opin Ophthalmol*. 2010;21(2):106–111.
27. Berdahl JP, Allingham RR, Johnson DH. Cerebrospinal fluid pressure is decreased in primary open-angle glaucoma. *Ophthalmology*. 2008;115(5):763–768.
28. Berdahl JP, Ethier CR, Allingham RR. Cerebrospinal fluid pressure and glaucomatous optic disc cupping. *Graefes Arch Clin Exp Ophthalmol*. 2009;247(9):1289–1290; author reply 1291–1284.
29. Berdahl JP, Fautsch MP, Stinnett SS, Allingham RR. Intracranial pressure in primary open angle glaucoma, normal tension glaucoma, and ocular hypertension: a case-control study. *Invest Ophthalmol Vis Sci*. 2008;49(12):5412–5418.
30. Berdahl JP, Yu DY, Morgan WH. The translaminar pressure gradient in sustained zero gravity, idiopathic intracranial hypertension, and glaucoma. *Med Hypotheses*. 2012;79(6):719–724.
31. Morgan WH, Balaratnasingam C, Cringle SJ, Yu DY. Glaucoma and cerebrospinal fluid pressure. *Ophthalmology*. 2008;115(12):2317–2318; author reply 2318.
32. Morgan WH, Chauhan BC, Yu DY, Cringle SJ, Alder VA, House PH. Optic disc movement with variations in intraocular and cerebrospinal fluid pressure. *Invest Ophthalmol Vis Sci*. 2002;43(10):3236–3242.
33. Morgan WH, Yu DY, Alder VA, et al. The correlation between cerebrospinal fluid pressure and retrolaminar tissue pressure. *Invest Ophthalmol Vis Sci*. 1998;39(8):1419–1428.
34. Morgan WH, Yu DY, Balaratnasingam C. The role of cerebrospinal fluid pressure in glaucoma pathophysiology: the dark side of the optic disc. *J Glaucoma*. 2008;17(5):408–413.
35. Morgan WH, Yu DY, Cooper RL, Alder VA, Cringle SJ, Constable IJ. The influence of cerebrospinal fluid pressure on the lamina cribrosa tissue pressure gradient. *Invest Ophthalmol Vis Sci*. 1995;36(6):1163–1172.
36. Hua Y, Voorhees AP, Sigal IA. Cerebrospinal fluid pressure: revisiting factors influencing optic nerve head biomechanics. *Invest Ophthalmol Vis Sci*. 2018;59(1):154–165.
37. Ren R, Jonas JB, Tian G, et al. Cerebrospinal fluid pressure in glaucoma: a prospective study. *Ophthalmology*. 2010;117(2):259–266.
38. Yang D, Fu J, Hou R, et al. Optic neuropathy induced by experimentally reduced cerebrospinal fluid pressure in monkeys. *Invest Ophthalmol Vis Sci*. 2014;55(5):3067–3073.
39. Killer HE, Flammer J, Miller NR. Glaucoma and cerebrospinal fluid pressure. *Ophthalmology*. 2008;115(12):2316–2317; author reply 2317.
40. Liu KC, Fleischman D, Lee AG, Killer HE, Chen JJ, Bhatti MT. Current concepts of cerebrospinal fluid dynamics and the translaminar cribrosa pressure gradient: a paradigm of optic disk disease. *Surv Ophthalmol*. 2020;65(1):48–66.
41. Wostyn P, De Groot V, Van Dam D, Audenaert K, Killer HE, De Deyn PP. Glaucoma and the role of cerebrospinal fluid dynamics. *Invest Ophthalmol Vis Sci*. 2015;56(11):6630–6631.
42. Feola AJ, Coudrillier B, Mulvihill J, et al. Deformation of the lamina cribrosa and optic nerve due to changes in cerebrospinal fluid pressure. *Invest Ophthalmol Vis Sci*. 2017;58(4):2070–2078.
43. Fleischman D, Berdahl JP, Zaydlarova J, Stinnett S, Fautsch MP, Allingham RR. Cerebrospinal fluid pressure decreases with older age. *PLoS One*. 2012;7(12):e52664.
44. Turner DC, Edmiston AM, Zohner YE, et al. Transient intraocular pressure fluctuations: source, magnitude, frequency, and associated mechanical energy. *Invest Ophthalmol Vis Sci*. 2019;60(7):2572–2582.
45. Jasien JV, Samuels BC, Johnston JM, Downs JC. Diurnal cycle of translaminar pressure in nonhuman primates quantified with continuous wireless telemetry. *Invest Ophthalmol Vis Sci*. 2020;61(2):37.
46. Chan TV, Vese LA. Active contours without edges. *IEEE Trans Image Process*. 2001;10(2):266–277.

47. Magnaes B. Body position and cerebrospinal fluid pressure. Part 1: clinical studies on the effect of rapid postural changes. *J Neurosurg*. 1976;44(6):687–697.
48. Hou R, Zhang Z, Yang D, et al. Intracranial pressure (ICP) and optic nerve subarachnoid space pressure (ONSP) correlation in the optic nerve chamber: the Beijing Intracranial and Intraocular Pressure (iCOP) study. *Brain Res*. 2016;1635:201–208.
49. Eklund A, Johannesson G, Johansson E, et al. The pressure difference between eye and brain changes with posture. *Ann Neurol*. 2016;80(2):269–276.
50. Kwun Y, Han JC, Kee C. Comparison of lamina cribrosa thickness in normal tension glaucoma patients with unilateral visual field defect. *Am J Ophthalmol*. 2015;159(3):512–518.e1.
51. Krzyzanowska-Berkowska P, Czajor K, Syga P, Iskander DR. Lamina cribrosa depth and shape in glaucoma suspects. comparison to glaucoma patients and healthy controls. *Curr Eye Res*. 2019;44(9):1026–1033.